Kasahara, J., Stephen, R.A., Acton, G.D., and Frey, F.A. (Eds.)
Proceedings of the Ocean Drilling Program, Scientific Results Volume 200

2. Data Report: Petrological and Geochemical Features of Igneous Basement at Site 1224[1]

Satoru Haraguchi[2] and Teruaki Ishii[2]

ABSTRACT

During Ocean Drilling Program Leg 200, ~45 Ma igneous basement, was cored in the northeastern Pacific at Site 1224. The basement surface was inferred to be 28 meters below seafloor (mbsf). Basement lithology down to 170 mbsf is divided into three major units: Unit 1 = massive flow, Unit 2 = pillow breccia, and Unit 3 = intermixed pillows and thin flows.

The bulk compositions of Site 1224 rocks have high abundances of the high-field strength elements (HFSE) Y, Zr, and Nb relative to normal and even enriched mid-ocean-ridge basalts. Chemical stratigraphic differences among the three units at this site are clear. Unit 3 rocks have the highest FeO/MgO ratio and HFSE concentration, and Unit 2 lavas have the lowest. Unit 2 lavas also have the highest Y/Zr ratios. Unit 1 is separated into lower and upper flow units based on differences in HFSE content. Clearly, there were significant differences in the petrogenetic processes that created these units.

Compositional and lithologic differences among the basement units correlate with differences in physical properties among the units described by the Leg 200 Shipboard Scientific Party. Physical properties are therefore associated with petrological features.

INTRODUCTION

Site 1224, at the Hawaii-2 observatory in the northeastern Pacific Ocean (Fig. F1), is situated west of isochron 20 (45 Ma) and was formed

F1. Location map, p. 7.

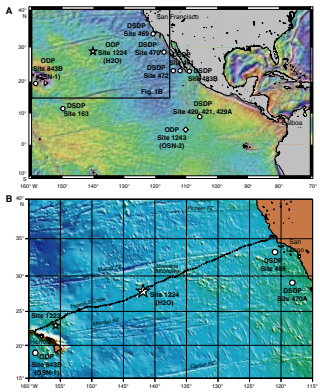

[1] Haraguchi, S., and Ishii, T., 2006. Petrological and geochemical features of igneous basement at Site 1224. *In* Kasahara, J., Stephen, R.A., Acton, G.D., and Frey, F.A. (Eds.), *Proc. ODP, Sci. Results,* 200, 1–19 [Online]. Available from World Wide Web: <http://www-odp.tamu.edu/publications/200_SR/VOLUME/CHAPTERS/002.PDF>. [Cited YYYY-MM-DD]
[2] Ocean Research Institute, University of Tokyo, 1-15-1, Minamidai, Nakano, Tokyo, 164-8639, Japan. Correspondence author: haraguti@ori.u-tokyo.ac.jp

Initial receipt: 21 May 2004
Acceptance: 14 February 2006
Web publication: 22 June 2006
Ms 200SR-002

between the Pacific and Farallon plates at a fast half-rate of ~71 mm/yr (Atwater, 1989; Cande and Kent, 1992).

In the northeastern Pacific Ocean, Deep Sea Drilling Project (DSDP) and Ocean Drilling Program (ODP) operations have recovered igneous basement at few sites. Only three DSDP and ODP holes penetrated >100 m into igneous basement—DSDP Leg 65 Hole 483B; ODP Leg 203 Hole 1243A, and ODP Leg 200 Hole 1224F—although several other sites have penetrated <100 m of igneous basement (Shipboard Scientific Party, 2003a, 2003b) (Fig. **F1,** Table **T1**). Therefore, studies of igneous basement at Site 1224 are critical to constrain the temporal and geographical variation of mid-ocean volcanism at the East Pacific Rise.

T1. Holes with penetration >10 m, p. 17.

LITHOLOGY

At Site 1224, basaltic basement was recovered from four holes (Holes 1224A, 1224D, 1224E, and 1224F) out of the six that were drilled. At this site the top of igneous basement was inferred to be at 28 meters below seafloor (mbsf). Igneous basement down to 170 mbsf is divided into three lithostratigraphic units: Unit 1 = massive flow, Unit 2 = pillow breccia, and Unit 3 = intermixed pillows and thin flows (Shipboard Scientific Party, 2003a) (Fig. **F2**).

F2. Lithologic summary of igneous basements, p. 8.

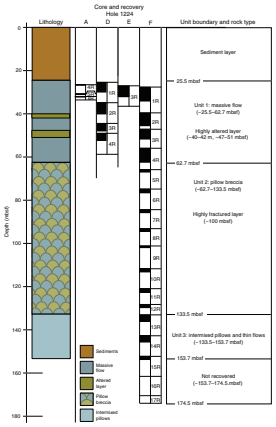

At Site 1224, basaltic basement was recovered from four holes (Holes 1224A, 1224D, 1224E, and 1224F) out of the six that were drilled. At this site the top of igneous basement was inferred to be at 28 meters below seafloor (mbsf). Igneous basement down to 170 mbsf is divided into three lithostratigraphic units: Unit 1 = massive flow, Unit 2 = pillow breccia, and Unit 3 = intermixed pillows and thin flows (Shipboard Scientific Party, 2003a) (Fig. **F2**).

Cores from Unit 1, the shallowest unit, had recovery of 30%–50%. This unit shows massive structure with some altered layers and vein deposits. The primary mineral phases are plagioclase, clinopyroxene, opaque minerals, and rare pigeonite. The majority of the basalt is holocrystalline to hypocrystalline lava flows. This unit is divided into two thick lava flows based on grain size, stratigraphy, and alteration layers.

Intermediate-depth Unit 2 differs from Unit 1; however, core recovery was so low (<10%) that the characteristics of the in situ rock are difficult to describe. Many of the small pieces retain almost circumferential alteration halos and thus were not significantly rounded by churning of rubble broken from the hole by the bit. Several pieces still retain fresh or altered glass, most probably representing pieces of chilled margins of pillow lava. Some calcite-cemented hyaloclastite layers were also found. The difference in induration between Units 1 and 2 is so great that the drill bit broke at the boundary.

Unit 3, the deepest unit, shows features similar to Unit 1. Fracture and alteration patterns are similar to those of Unit 1, with reddish brown stains forming halos on small pieces and parallel fractures lined with iron oxyhydroxides and calcite in larger pieces. Portions of at least two cooling units were recovered, possibly more. Recovery in Unit 3 was lower than that in Unit 1 but higher than that in Unit 2 (~20%–30%).

ANALYTICAL METHODS

Bulk rock compositions were determined for 51 samples from Site 1224 using a Rigaku 3270 X-ray fluorescence (XRF) spectrometer at the Ocean Research Institute, University of Tokyo, Japan. Major element analyses were conducted using glass beads. Samples were cut into slabs, washed with distilled water, and finely ground in an agate ball mill. One gram of powdered sample was dried at 110°C for ~10 hr and weighed to obtain weight percent H_2O loss. The dried samples were then ignited at 950°C for ~4 hr and weighed to obtain loss on ignition

(LOI). Fused disks were prepared with a lithium tetraborate ($Li_2B_4O_7$) flux at a dilution ratio of 1:10. Trace element analyses were performed using pressed powder pellets (~4 g of sample) made with a polyvinyl acetate ring holder (after Goto and Tatsumi, 1991). XRF major and trace element data are presented in Table T2.

Mineral phases were analyzed using a JEOL-733 electron microprobe also at the Ocean Research Institute, Japan, using 15-kV accelerating potential, 1.2×10^8 A sample current, 1-µm beam diameter, and natural mineral standards (Bence and Albee 1968; Nakamura and Kushiro 1970).

T2. XRF analysis, p. 18.

RESULTS AND DISCUSSION

Bulk Rock Alteration

All samples analyzed were selected to exclude obvious signs of alteration (i.e., veined material); however, some alteration characteristics, such as brown color, were observed in the rocks, especially those from Units 2 and 3.

The effect of alteration on the bulk rock chemistry of pillow basalts have been studied extensively in Hole 504B (e.g., Kempton et al., 1985; Sparks, 1995). They concluded that K and Sr are mobile in the upper pillow section where seawater interaction is greatest. Emmermann (1985) divided alteration in pillow lavas into upper oxidative and lower nonoxidative zones, with K, S, and iron oxidation ratios being the most effective discrimination measures between these zones.

Fig. F3A shows LOI vs. $H_2O(-)$ for Site 1224 rocks. Many samples, especially those from Unit 1, show negative LOI results. This characteristic indicates that the weight increase arising from oxidation of Fe^{2+} to Fe^{3+} (FeO to Fe_2O_3) is higher than the weight loss caused by removing volatiles from the mineral structures. All samples have low $H_2O(-)$ (<1.4 wt%) and LOI (<0.8 wt%). Fig. F3B is K_2O vs. $H_2O(-)$. Some samples with high water content show high K_2O. However, K_2O content does not increase with increasing water content (Fig. F3B). We therefore considered the Site 1224 rocks to show a low degree of alteration. Nevertheless, we recognize that K and Rb contents were affected by alteration processes.

F3. $H_2O(-)$ vs. loss on ignition and K_2O vs. $H_2O(-)$, p. 9.

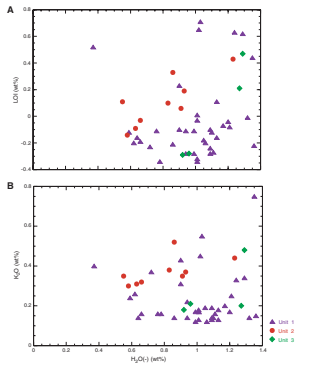

Major and Trace Element Geochemistry

In Site 1224 basalt, SiO_2 ranges from 48 to 53 wt% as MgO varies over narrow range of 5 to 7 wt% (Fig. F4A). FeO/MgO ratios of rocks from all three units are higher (1.3–3.0) than typical mid-ocean-ridge basalt (MORB) ratios, which are normally 1–1.5. Unit 2 has the lowest (1.2–1.8), Unit 3 has the highest (2.3–3.0), and Unit 1 has intermediate (1.6–2.6) (Fig. F4A).

Site 1224 rocks show interesting trace element characteristics (Fig. F4B). Most compatible and incompatible trace elements of the three units overlap, and they do not show clear crystal fractionation trends. However, the HFSE (e.g., Y, Zr, and Nb) compositions of the three units are remarkably different: Unit 2 has the lowest concentration, Unit 3 has the highest, and two different concentrations are observed in Unit 1.

The most important trace element characteristic is that Site 1224 rocks have higher HFSE content than typical normal (N-) and enriched (E-) MORB, as compiled by Sun and McDonough (1989). Y and Zr con-

F4. Major and trace elements vs. MgO, p. 10.

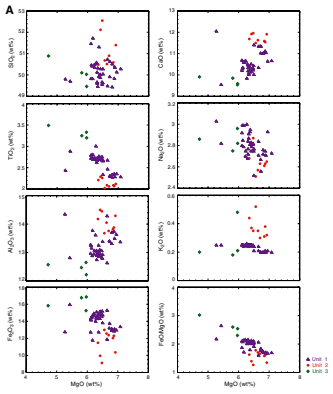

centrations are two to three times higher than those of N- and E-MORB, and Y is nearly twice that of oceanic island basalt (OIB) (Fig. F5A). The average Y/Zr ratios in these rocks are similar to that in E-MORB. In detail, Unit 2 has a slightly higher ratio than the other two units. This higher Y/Zr ratio for Unit 2 at similar Y and Zr content reflects a different petrogenesis for this unit. It is likely that the high trace element contents of these rocks are a result of extensive crystal fractionation.

Chemostratigraphy

Significant chemical stratigraphic (chemostratigraphic) differences among the three units at Site 1224 are clearly shown in element concentration vs. depth diagrams (Fig. F6). The highest FeO/MgO ratios and abundances of TiO_2, Y, Zr, and Nb are in Unit 3; the lowest are in Unit 2, which also has the highest Y/Zr. Also, the two flows in Unit 1 are indicated by abrupt downhole decreases in abundance of TiO_2, Y, Zr, and Nb.

It is important to note that each lithologic unit has different *P*-wave velocity, bulk density, and other physical properties (Shipboard Scientific Party, 2003a). It is thought that physical properties are associated with lithologic features (massive flows and breccia, degree of alteration, etc.).

Mineral Chemistry

At Site 1224, plagioclase and clinopyroxene are the major mineral phases, and they are potential fractionating phases. Clinopyroxene groundmass composition is consistent with bulk composition; that is, groundmass clinopyroxene in Unit 2 has higher Mg# than in Unit 3 (Fig. F7). In contrast, these units have no systematic differences in their plagioclase groundmass compositions (anorthite content= 40–70; mean = ~60).

Petrogenesis

As a group, Site 1224 basalts display positive correlation between abundances of the incompatible trace elements Y, Zr, and Nb and the FeO/MgO ratio and negative correlations between FeO/MgO and Sr, Ni, and Cr (Fig. F8), which are compatible in plagioclase, olivine, and clinopyroxene, respectively.

Sun and McDonough (1989) compiled chemical data for N-MORB, E-MORB, and OIB and published typical compositions of these basalts. Studies of basalt from deep basements on the Costa Rica Rift (Hole 504B and Leg 148) showed that the compositional variation of these basalts dominantly reflect crystal fractionation (e.g., Brewer et al., 1996). In comparison, Site 1224 basalt is much more evolved (FeO/MgO of 1.3–3.0), and abundances of Zr and Y are higher by a factor of two. Clearly, Site 1224 lavas experienced unusually large amounts of crystal fractionation within the crust.

SUMMARY AND CONCLUSIONS

1. Basement at Site 1224 is separated into three lithologic units: Unit 1 (massive flow; ~26–62 mbsf), Unit 2 (pillow breccia; ~62–135 mbsf), and Unit 3 (intermixed pillow and thin flows; ~135

F5. Y vs. Zr and Rb vs. Sr, p. 12.

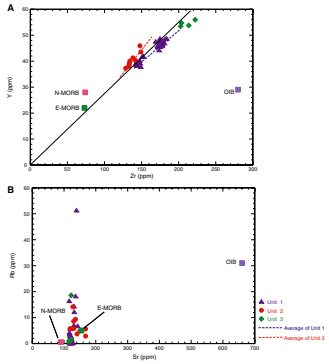

F6. Major elements and FeO/MgO, trace elements and Y/Zr, p. 13.

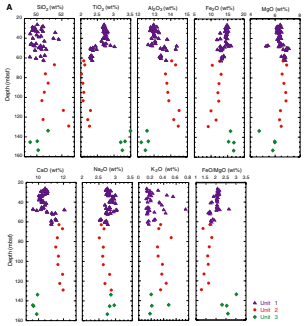

F7. Clinopyroxene groundmass, p. 15.

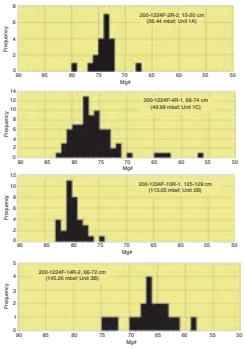

F8. Major elements, trace elements, and element ratios vs. FeO/MgO, p. 16.

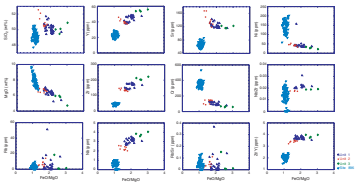

mbsf). Unit 1 is divided into two subunits (upper and lower flow units) based on grain size of groundmass and distribution of alteration halos. Unit 2 is divided into two subunits based on recovery and differences in alteration effects.

2. Differences in HFSE and compositions among the three units are remarkable. Unit 3 has the highest content of these elements, and Unit 2 has the lowest. Units 1 and 2 are divided into two subunits on the basis of these elements, and this classification is consistent with lithologic characteristics. It is thought that these chemical differences reflect differentiation process (i.e., fractionation of clinopyroxene).
3. Variations in physical properties and downhole logging data correspond to the lithologic and chemostratigraphic changes that define the units and subunits.
4. The basement rocks have high incompatible element contents (e.g., higher HFSE content than N-MORB), and some element contents are similar to OIB (cf. Sun and McDonough., 1989). Based on their high abundances of immobile HFSE (Zr and Y) and high, MORB-like Zr/Nb, we conclude that these are MORB that fractionated the mineral phases, olivine, clinopyroxene, and plagioclase within the oceanic crust.

ACKNOWLEDGMENTS

We recognize the major contributions of J. Kasahara, R. Stephen, and other shipboard scientists; marine technicians; and the crew of the *JOIDES Resolution* to the success of drilling efforts at Site 1224. This research used samples and/or data supplied by the Ocean Drilling Program (ODP). ODP is sponsored by the U.S. National Science Foundation (NSF) and participating countries under management of Joint Oceanographic Institutions (JOI), INC. Funding of this research was provided by Grant-in-Aid No. 14340147 from the Ministry of Education, Science, Sports and Culture, Japan.

REFERENCES

Atwater, T., 1989. Plate tectonic history of the northeast Pacific and western North America. *In* Winterer, E.L., Hussong, D.M., and Decker, R.W. (Eds.), *The Eastern Pacific Ocean and Hawaii*. Geol. Soc. Am., Geol. of North America Ser., N:21–72.

Bence, A.E., and Albee, A.L., 1968. Empirical correction factors for the electron microanalysis of silicates and oxides. *J. Geol.,* 76:382–403.

Brewer, T.S., Bach, W., and Furnes, H., 1996. Geochemistry of lavas from Hole 896A. *In* Alt, J.C., Kinoshita, H., Stokking, L.B., and Michael, P.J. (Eds.), *Proc. ODP, Sci. Results,* 148: College Station, TX (Ocean Drilling Program), 9–19.

Cande, S.C., and Kent, D.V., 1992. A new geomagnetic polarity time scale for the Late Cretaceous and Cenozoic. *J. Geophys. Res.,* 97(10):13917–13951.

Emmermann, R., 1985. Basement geochemistry, Hole 504B. *In* Anderson, R.N., Honnorez, J., Becker, K., et al., *Init. Repts. DSDP,* 83: Washington (U.S. Govt. Printing Office), 183–199.

Fryer, P., Pearce, J.A., Stokking, L.B., et al., 1990. *Proc. ODP, Init. Repts.,* 125: College Station, TX (Ocean Drilling Program).

Goto, T., and Tatsumi, Y., 1991. Quantitative analysis of rock samples using X-ray fluorescence analyzer. *Rigaku Janaru,* 22:28–44.

Kempton, P.D., Autio, L.K., Rhodes, J.M., Holdaway, M.J., Dungan, M.A., and Johnson, P., 1985. Petrology of basalts from Hole 504B, Deep Sea Drilling Project, Leg 83. *In* Anderson, R.N., Honnorez, J., Becker, K., et al., *Init. Repts. DSDP,* 83: Washington (U.S. Govt. Printing Office), 129–164.

Nakamura, Y., and Kushiro, I., 1970. Compositional relations of coexisting orthopyroxene, pigeonite, and sugite in a tholeiitic andesite from Hakone volcano. *Contrib. Mineral. Petrol.,* 26:265–275. **doi:10.1007/BF00390075**

Shipboard Scientific Party, 2003a. Leg 200 summary. *In* Stephen, R.A., Kasahara, J., Acton, G.D., et al., *Proc. ODP, Init. Repts.,* 200: College Station TX (Ocean Drilling Program), 1–72. [**HTML**]

Shipboard Scientific Party, 2003b. Leg 203 summary. *In* Orcutt, J.A., Schultz, A., Davies, T.A., et al., *Proc. ODP, Init. Repts.,* 203: College Station TX (Ocean Drilling Program), 1–30. [**HTML**]

Sparks, J.W., 1995. Geochemistry of the lower sheeted dike complex, Hole 504B, Leg 140. *In* Erzinger, J., Becker, K., Dick, H.J.B., and Stokking, L.B. (Eds.), *Proc. ODP, Sci. Results,* 137/140: College Station, TX (Ocean Drilling Program), 81–98.

Sun, S.-S., and McDonough, W.F., 1989. Chemical and isotopic systematics of oceanic basalts: implications for mantle composition and processes. *In* Saunders, A.D., and Norry, M.J. (Eds.), *Magmatism in the Ocean Basins*. Geol. Soc. Spec. Publ., 42:313–345.

Figure F1. A, B. Location maps showing Site 1224 (Hawaii-2 Observatory [H2O]; star), Site 1243 (Ocean Seismic Network [OSN]-2; diamond), and previous drill sites with penetration >10 m into Pacific crust (circles) (modified from Shipboard Scientific Party, 2003b [A], 2003a [B]). FZ = fracture zone.

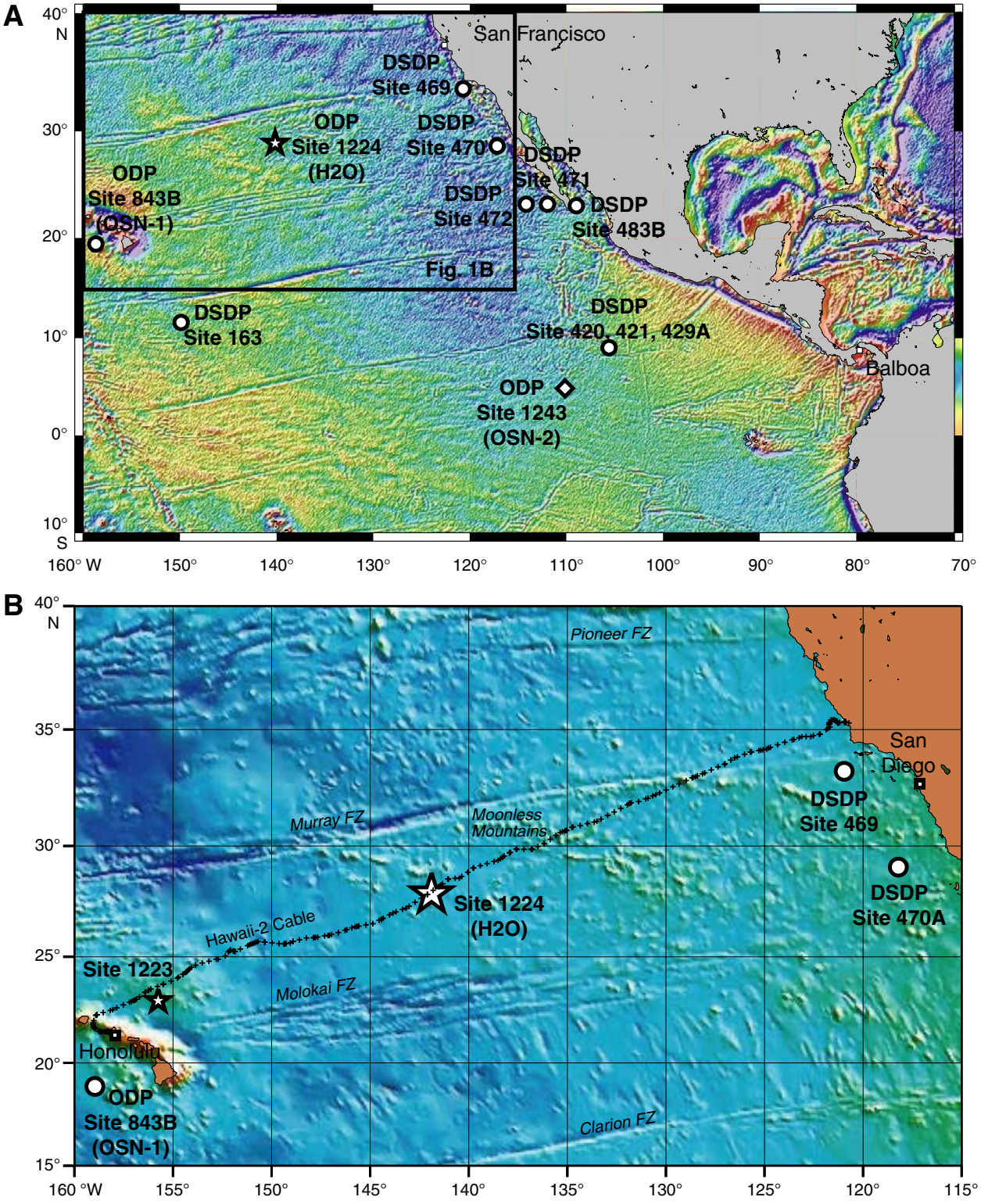

Figure F2. Lithologic summary of igneous basements cored at Site 1224 (modified from Fryer, Pearce, Stokking, et al., 1990).

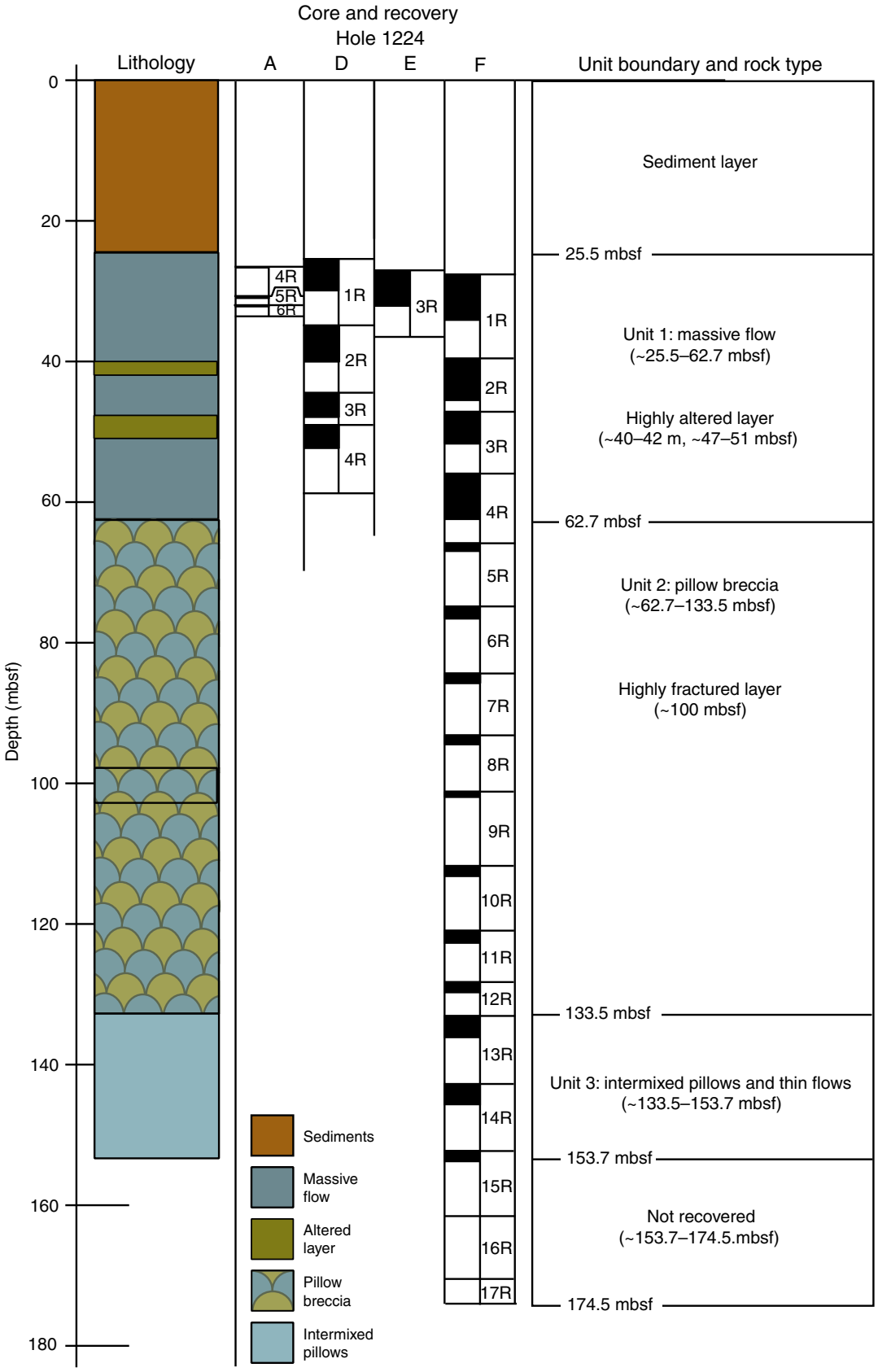

Figure F3. (**A**) $H_2O(-)$ vs. loss on ignition (LOI) and (**B**) K_2O vs. $H_2O(-)$ for Site 1224 rocks.

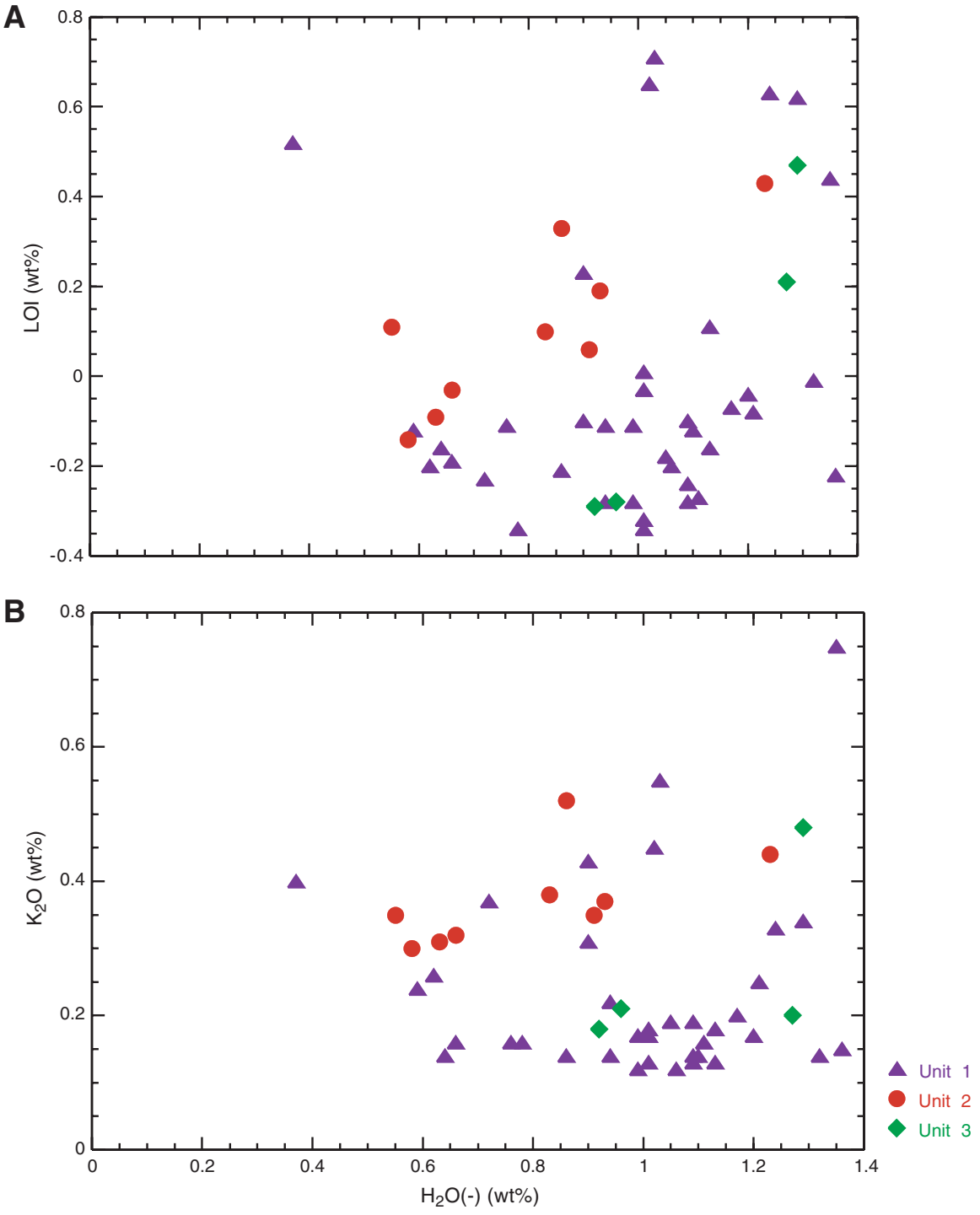

Figure F4. A. Major elements vs. MgO for Site 1224 rocks. (Continued on next page.)

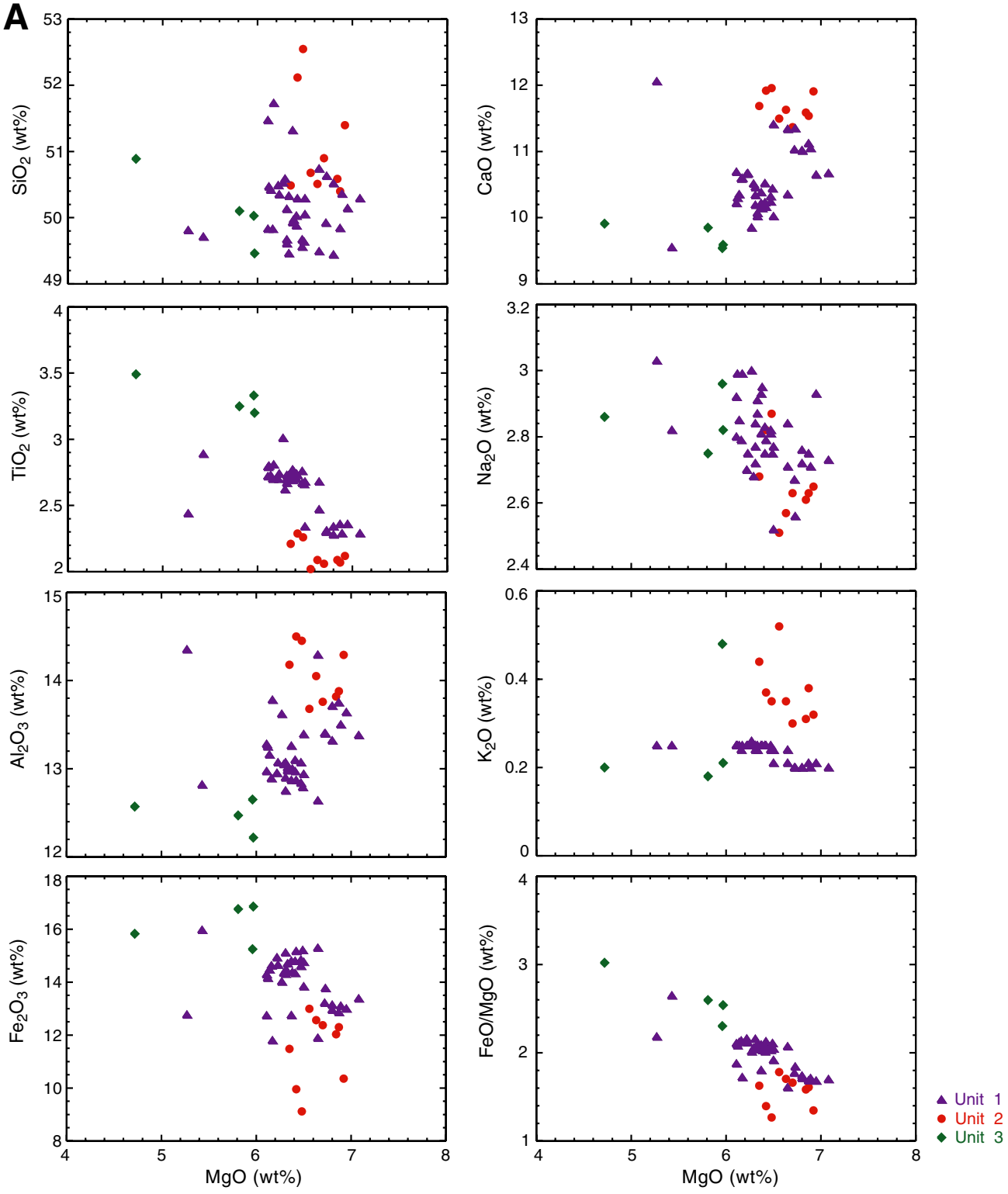

Figure F4 (continued). **B.** Trace elements vs. MgO for Site 1224 rocks.

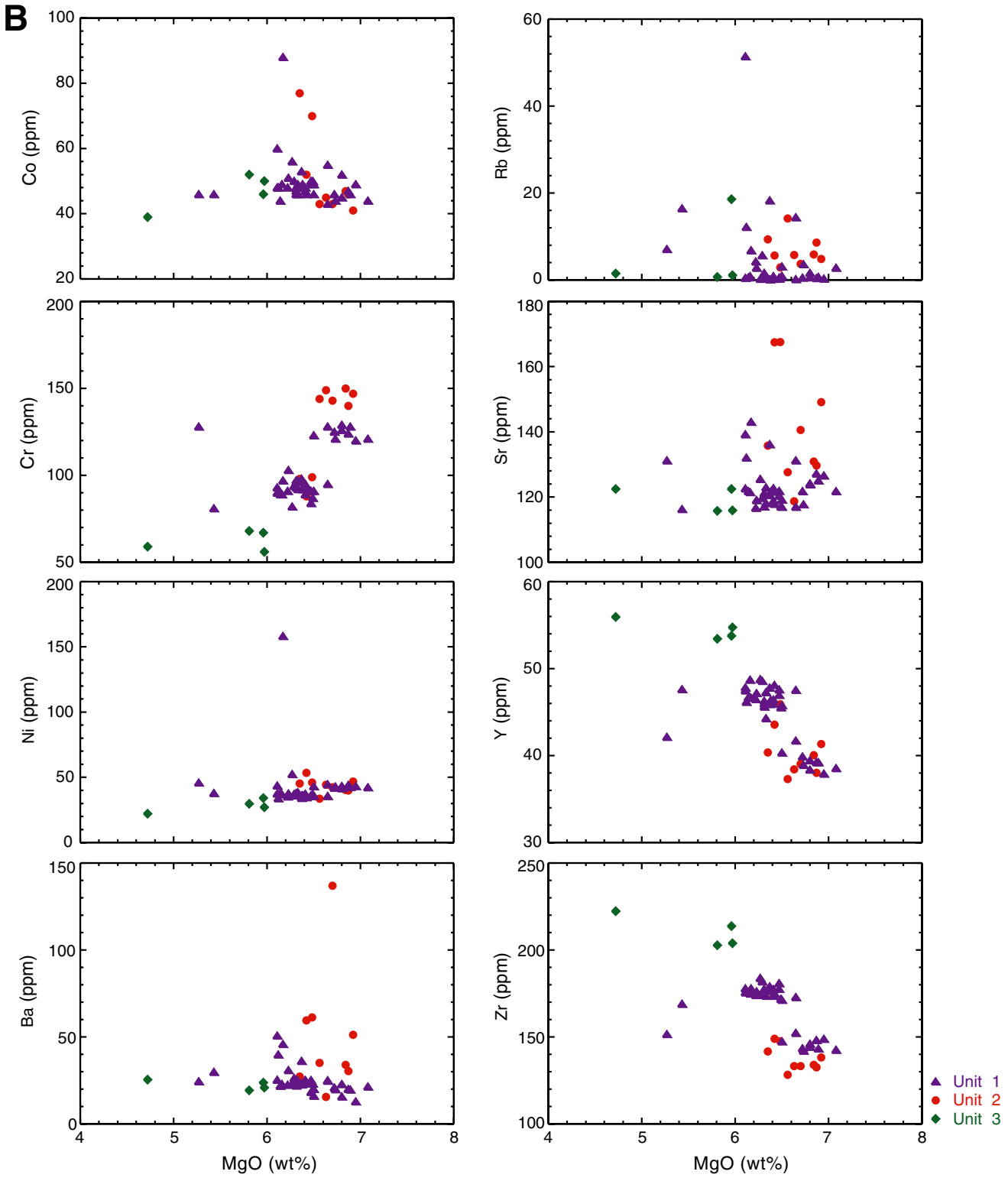

Figure F5. (**A**) Y vs. Zr and (**B**) Rb vs. Sr for Site 1224 rocks compared with typical compositions of normal mid-ocean-ridge basalt (N-MORB), enriched MORB (E-MORB), and oceanic island basalt (OIB) (Sun and McDonough, 1989).

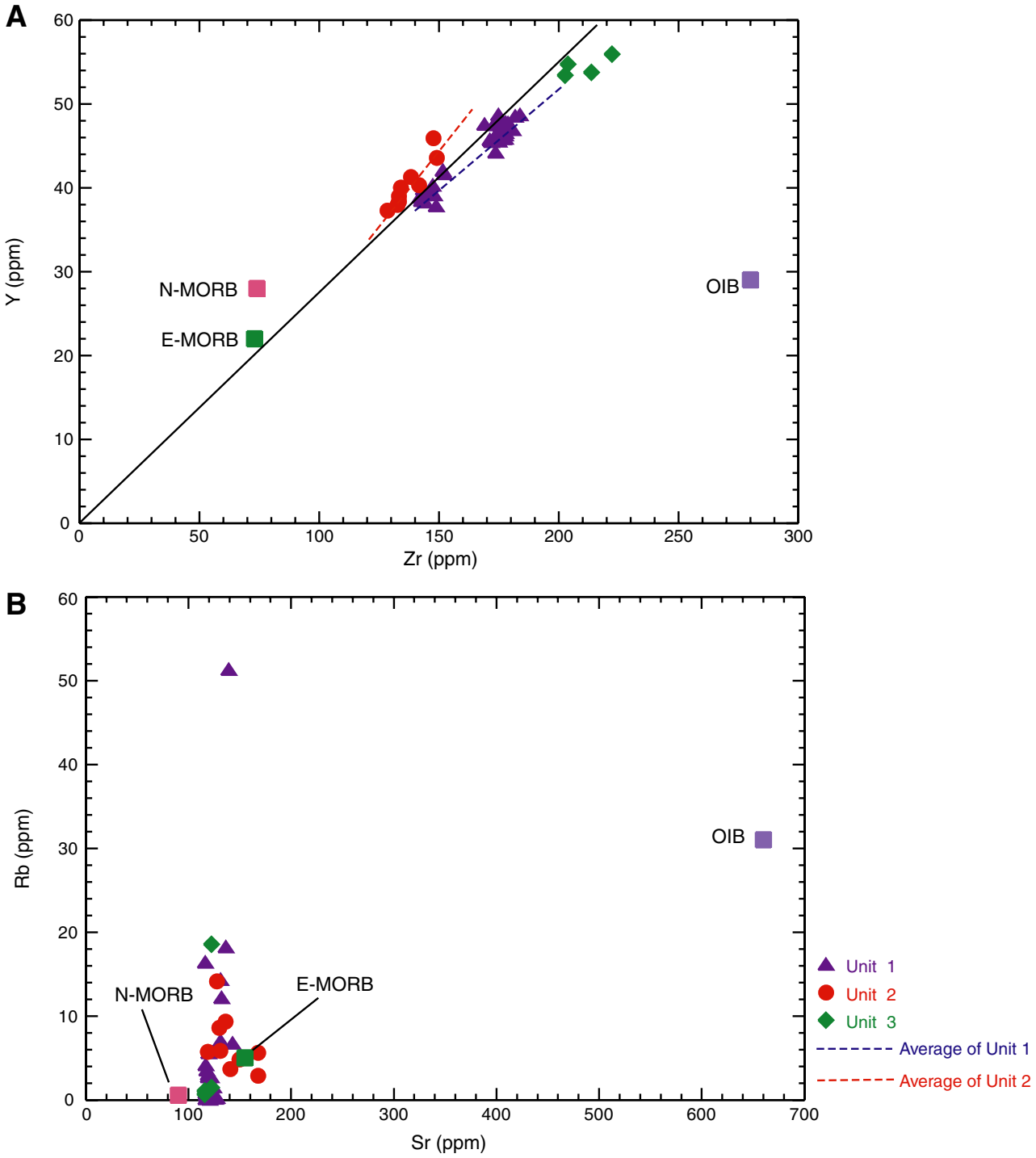

Figure F6. A. Downhole variations of major elements and FeO/MgO at Site 1224. (Continued on next page.)

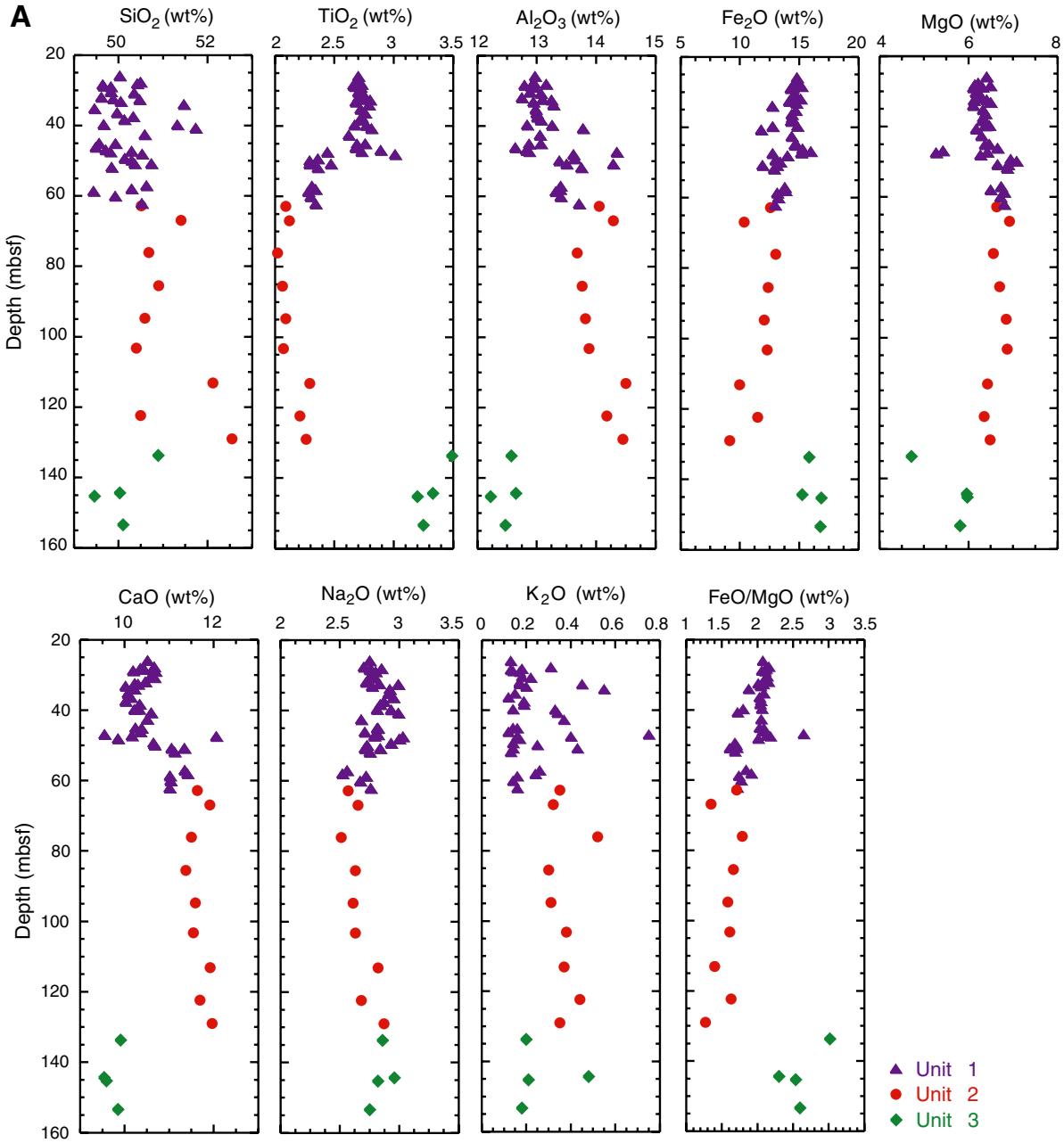

Figure F6 (continued). **B.** Downhole variations of trace elements and Y/Zr at Site 1224.

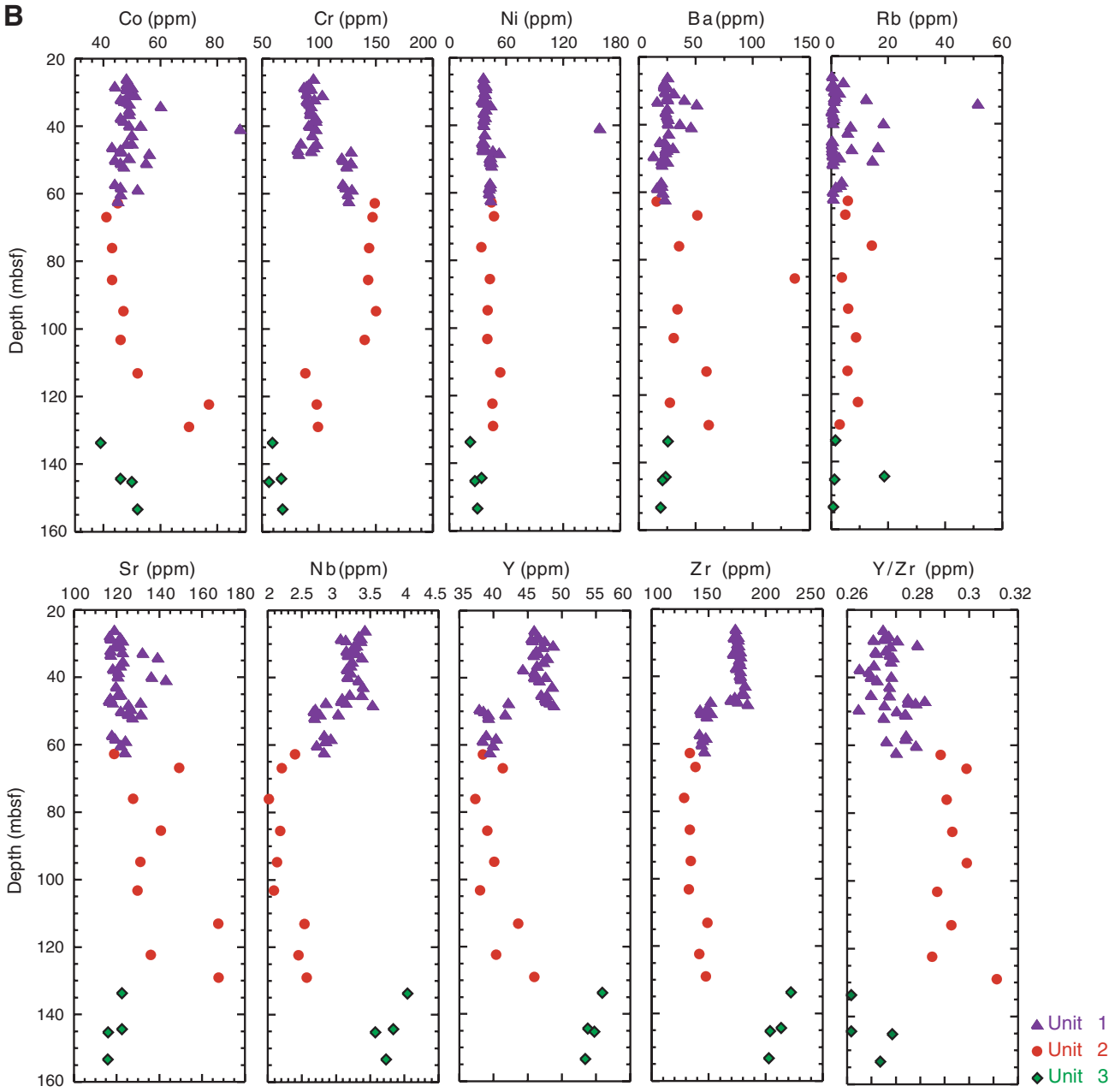

Figure F7. Core compositions of clinopyroxene groundmass in Site 1224 rocks from the upper and lower subunits in Units 1, 2, and 3.

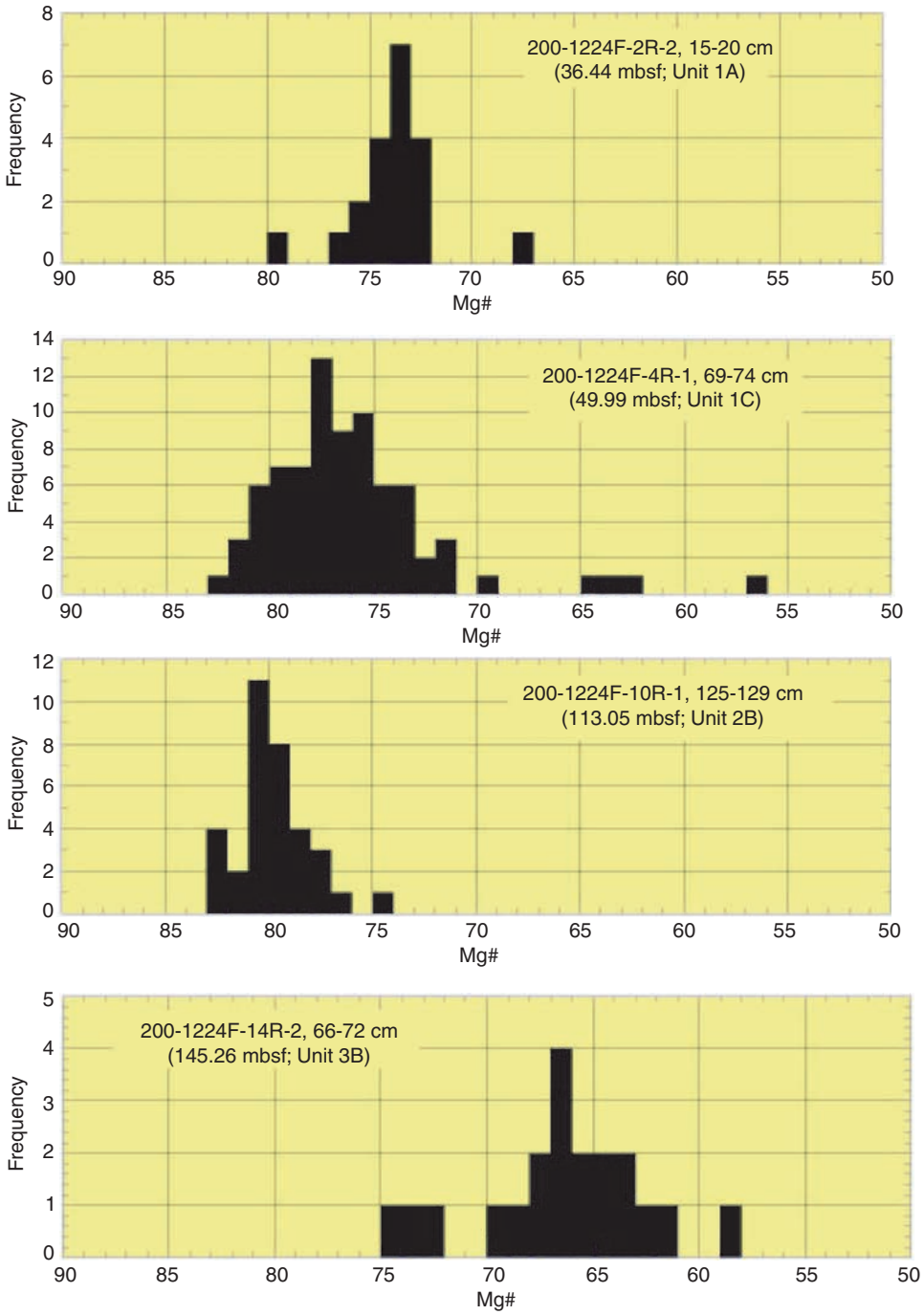

Figure F8. Major elements, trace elements, and element ratios vs. FeO/MgO for Site 1224 rocks compared with typical depleted MORB in the Costa Rica ridge, Site 896, ODP Leg 148 (Brewer, 1996).

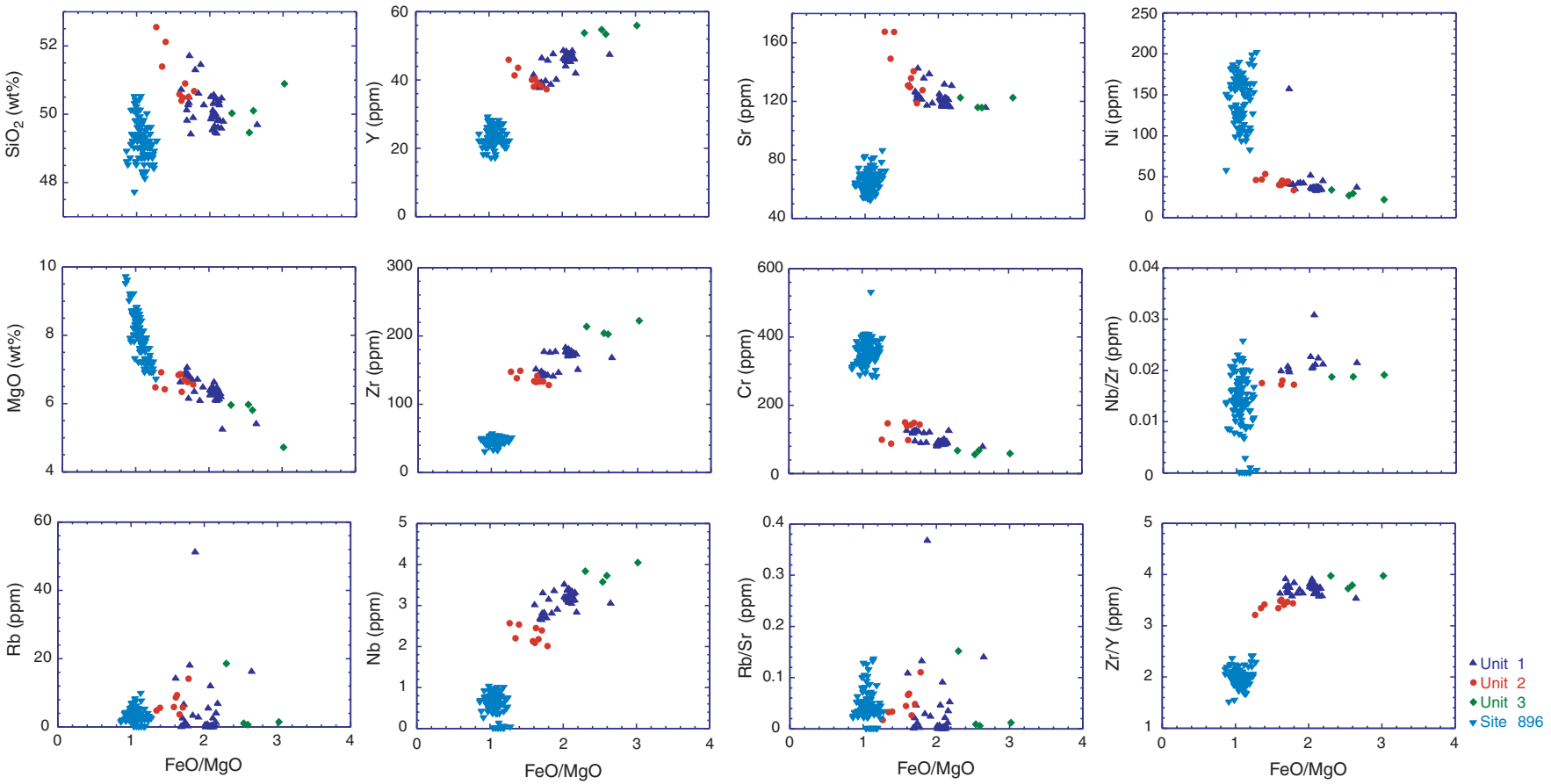

Table T1. Summary of DSDP and ODP holes in Pacific crust with penetration >10 m.

Leg	Site/ Hole	Age (Ma)	Latitude	Longitude	Basement penetration (m)	Sediment thickness (m)
DSDP 16	163	72	11°15′N	150°18′W	18	176
DSDP 54	420	3.4	09°01′N	106°06′W	29	118
DSDP 54	421	3.4	09°01′N	106°04′W	29	85
DSDP 54	429A	4.6	09°02′N	106°46′W	21	31
DSDP 63	469	17	32°37′N	120°33′W	58	391
DSDP 63	470A	15	28°54′N	117°31′W	48	167
DSDP 63	471	12	23°29′N	112°30′W	82	741
DSDP 63	472	15	23°00′N	114°00′W	25	112
DSDP 65	483B	1.7	22°53′N	108°45′W	157	110
DSDP 92	597B	29	18°48′S	129°46′W	25	48
DSDP 92	597C	29	18°48′S	129°46′W	91	53
DSDP 92	599B	8	19°27′S	119°53′W	10	41
ODP 136	843B	95	19°21′N	159°06′W	71	243
ODP 200	1224D	46	27°53′N	141°59′W	36	29
ODP 200	1224F	46	27°53′N	141°59′W	145	29
ODP 203	1243A	12	05°18′N	110°05′W	107	117
ODP 203	1243B	12	05°18′N	110°04′W	85	113

Table T2. Major and trace element XRF analysis of Site 1224 basalts. (Continued on next page.)

Core, section, interval (cm)	Depth (mbsf)	Major element by XRF (wt%)												
		SiO_2	TiO_2	Al_2O_3	Fe_2O_3	MnO	MgO	CaO	Na_2O	K_2O	P_2O_5	Total	$H_2O(-)$	LOI
200-1224A-														
5X-1, 14–22	30.84	50.35	2.74	13.07	14.65	0.21	6.23	10.67	2.75	0.22	0.25	101.14	0.94	–0.28
6N-1, 7–11	32.07	49.61	2.70	12.75	15.11	0.20	6.31	10.46	2.72	0.17	0.25	100.28	1.01	–0.32
200-1224D-														
1R-1, 51–57	26.01	50.03	2.70	12.97	14.80	0.19	6.41	10.52	2.75	0.13	0.25	100.73	1.09	–0.28
1R-2, 80–85	27.74	50.49	2.70	12.95	14.93	0.21	6.22	10.66	2.70	0.31	0.25	101.41	0.90	–0.10
1R-3, 16–23	28.26	50.42	2.73	13.16	14.47	0.18	6.14	10.35	2.85	0.18	0.25	100.73	1.13	–0.16
1R-3, 44–49	28.54	49.64	2.66	12.79	15.21	0.20	6.49	10.44	2.75	0.13	0.24	100.57	1.01	–0.34
1R-4, 6–10	29.05	49.83	2.72	12.97	14.29	0.20	6.11	10.69	2.80	0.17	0.25	100.01	1.01	–0.03
2R-1, 19–25	35.29	49.46	2.72	12.98	14.70	0.19	6.33	10.07	2.91	0.15	0.25	99.77	1.36	–0.22
2R-2, 15–20	36.44	49.97	2.76	13.00	14.38	0.17	6.38	10.14	2.95	0.12	0.25	100.11	1.06	–0.20
2R-2, 114–120	37.53	50.33	2.73	13.01	14.40	0.16	6.33	10.02	2.87	0.19	0.24	100.28	1.09	–0.10
2R-3, 70–76	38.41	50.13	2.73	13.07	14.31	0.17	6.31	10.34	2.84	0.19	0.25	100.32	1.05	–0.18
2R-4, 73–79	39.76	49.67	2.67	12.84	14.84	0.18	6.47	10.32	2.81	0.14	0.24	100.21	1.09	–0.24
3R-1, 52–54	45.22	49.93	2.69	12.87	14.80	0.19	6.37	10.38	2.81	0.16	0.25	100.44	1.11	–0.27
3R-2, 57–62	46.24	49.49	2.68	12.64	15.29	0.20	6.65	10.35	2.71	0.12	0.24	100.38	0.99	–0.28
3R-2, 126–132	46.96	49.71	2.89	12.82	15.97	0.15	5.43	9.55	2.82	0.75	0.25	100.34	1.35	0.44
3R-3, 41–50	47.55	49.81	2.44	14.35	12.77	0.16	5.27	12.06	3.03	0.40	0.25	100.54	0.37	0.52
4R-1, 12–19	49.42	50.14	2.36	13.64	13.00	0.15	6.95	10.65	2.93	0.14	0.21	100.17	1.32	–0.01
4R-1, 69–74	49.99	50.29	2.29	13.38	13.38	0.16	7.08	10.67	2.73	0.25	0.20	100.44	1.21	–0.08
4R-2, 28–34	50.90	50.36	2.29	13.50	13.10	0.17	6.89	11.05	2.71	0.14	0.20	100.40	0.94	–0.11
5R-1, 61–70	51.91	49.84	2.36	13.75	12.87	0.17	6.87	11.12	2.75	0.13	0.21	100.06	1.13	0.11
200-1224E-														
3R-2, 51–53	28.90	49.67	2.67	12.90	14.45	0.17	6.31	10.19	2.77	0.14	0.24	99.50	1.10	–0.12
200-1224F-														
1R-2, 133–136	30.47	49.83	2.70	12.89	14.62	0.21	6.16	10.59	2.79	0.18	0.24	100.23	1.01	0.01
1R-4, 46–49	32.55	49.88	2.74	13.10	14.34	0.17	6.41	10.23	2.83	0.17	0.25	100.13	0.99	–0.11
1R-4, 61–62	32.70	50.47	2.80	13.25	14.16	0.17	6.12	10.30	2.99	0.45	0.25	100.96	1.02	0.65
1R-4, 118–120	33.27	50.05	2.68	12.94	14.76	0.18	6.50	10.02	2.77	0.20	0.24	100.33	1.17	–0.07
1R-5, 57–59	34.09	51.47	2.79	13.28	12.74	0.17	6.11	10.22	2.92	0.55	0.25	100.49	1.03	0.71
2R-1, 14–17	39.84	51.32	2.77	13.26	12.75	0.16	6.37	10.22	2.93	0.33	0.25	100.36	1.24	0.63
2R-1, 91–93	40.81	51.73	2.81	13.78	11.80	0.15	6.17	10.60	2.99	0.34	0.25	100.63	1.29	0.62
2R-3, 10–12	42.72	50.59	2.62	13.05	14.35	0.20	6.29	10.51	2.68	0.37	0.25	100.91	0.72	–0.23
2R-4, 138–140	45.14	49.56	2.76	13.07	14.61	0.17	6.47	10.24	2.82	0.14	0.25	100.10	0.86	–0.21
3R-1, 10–13	47.40	50.29	2.73	12.87	15.17	0.18	6.42	10.16	2.79	0.16	0.25	101.01	0.78	–0.34
3R-1, 90–95	48.20	50.53	3.01	13.62	14.02	0.14	6.27	9.85	3.00	0.17	0.26	100.88	1.20	–0.04
3R-3, 90–93	50.93	50.74	2.47	14.29	11.89	0.16	6.65	11.34	2.84	0.43	0.21	101.03	0.90	0.23
4R-1, 75–77	57.15	50.63	2.31	13.40	13.77	0.20	6.73	11.35	2.56	0.26	0.20	101.38	0.62	–0.20
4R-2, 84–86	58.14	50.29	2.34	13.39	13.84	0.20	6.50	11.41	2.52	0.24	0.21	100.93	0.59	–0.12
4R-3, 1–3	58.81	49.44	2.28	13.32	13.14	0.17	6.80	11.02	2.72	0.16	0.20	99.24	0.76	–0.11
4R-3, 134–136	60.14	49.92	2.30	13.40	13.22	0.17	6.72	11.03	2.67	0.14	0.20	99.77	0.64	–0.16
4R-5, 120–122	62.21	50.52	2.34	13.71	12.95	0.16	6.80	11.01	2.76	0.16	0.20	100.61	0.66	–0.19
4R-6, 24–27	62.72	50.51	2.09	14.05	12.57	0.18	6.63	11.63	2.57	0.35	0.19	100.78	0.91	0.06
5R-1, 93–96	66.83	51.40	2.12	14.29	10.36	0.17	6.92	11.91	2.65	0.32	0.18	100.33	0.66	–0.03
6R-1, 97–99	75.97	50.68	2.02	13.68	13.00	0.19	6.56	11.50	2.51	0.52	0.18	100.83	0.86	0.33
7R-1, 97–99	85.47	50.90	2.06	13.76	12.38	0.18	6.70	11.37	2.63	0.30	0.18	100.48	0.58	–0.14
8R-1, 108–111	94.68	50.59	2.09	13.82	12.04	0.18	6.84	11.59	2.61	0.31	0.19	100.25	0.63	–0.09
9R-1, 46–49	103.16	50.40	2.07	13.88	12.30	0.18	6.87	11.54	2.63	0.38	0.19	100.43	0.83	0.10
10R-1, 125–129	113.05	52.12	2.29	14.50	9.96	0.17	6.42	11.92	2.82	0.37	0.19	100.77	0.93	0.19
11R-1, 119–122	122.29	50.49	2.21	14.18	11.48	0.18	6.35	11.69	2.68	0.44	0.19	99.90	1.23	0.43
12R-1, 46–48	128.96	52.55	2.26	14.45	9.12	0.17	6.48	11.96	2.87	0.35	0.20	100.40	0.55	0.11
13R-1, 22–24	133.74	50.89	3.49	12.57	15.83	0.19	4.72	9.91	2.86	0.20	0.31	100.97	1.27	0.21
14R-1, 114–116	144.34	50.03	3.33	12.65	15.25	0.17	5.96	9.54	2.96	0.48	0.30	100.66	1.29	0.47
14R-2, 66–72	145.26	49.46	3.20	12.22	16.85	0.20	5.97	9.59	2.82	0.21	0.29	100.80	0.96	–0.28
15R-1, 95–97	153.35	50.10	3.25	12.47	16.76	0.20	5.81	9.85	2.75	0.18	0.29	101.66	0.92	–0.29

Notes: Accuracy is calculated based on analysis of standard sample, mainly igneous rock standard samples of Geological Survey of Japan, as linear fit note accuracy. Accuracies of XRF analysis: SiO_2 = 0.27%, TiO_2 = 0.017%, Al_2O_3 = 0.23%, Fe_2O_3 = 0.11%, MnO = 0.0047%, MgO = 0.11%, CaO = 0.098%, Na_2O = 0.19%, K_2O = 0.038%, P_2O_5 = 0.0042%, Co = 2.7%, Cr = 18.0%, Ba = 4.1%, Nb = 14.3%, Ni = 9.3%, Pb = 17.6%, Rb = 18.2%, Sr = 1.9%, Th = 29.0%, Y = 2.4%, and Zr = 1.8%.

Table T2 (continued).

Core, section, interval (cm)	Depth (mbsf)	Trace element by XRF (ppm)										
		CO	CR	Ba	Nb	Ni	Pb	Rb	Sr	Th	Y	Zr
200-1224A-												
5X-1, 14–22	30.84	51	103	30.9	3.3	37.5	ND	2.8	119.1	0.3	47.2	176.2
6N-1, 7–11	32.07	46	96	24.9	3.2	36.6	1.2	1.6	117.1	0.6	46.3	174.1
200-1224D-												
1R-1, 51–57	26.01	48	95	25.2	3.4	36.1	0.8	0.3	118.9	1.3	46.0	173.6
1R-2, 80–85	27.74	48	91	22.4	3.3	35.2	0.4	4.2	116.7	0.9	46.5	174.0
1R-3, 16–23	28.26	44	89	21.9	3.4	38.4	0.0	0.5	121.8	1.0	46.7	175.7
1R-3, 44–49	28.54	50	87	23.1	3.1	37.1	ND	0.6	117.1	0.5	45.5	171.8
1R-4, 6–10	29.05	48	90	25.4	3.4	37.5	0.3	0.5	122.6	0.1	47.5	175.5
2R-1, 19–25	35.29	49	92	24.9	3.2	38.5	0.3	0.6	123.0	0.9	47.3	176.5
2R-2, 15–20	36.44	49	92	23.2	3.2	36.1	ND	ND	121.6	0.9	46.4	177.7
2R-2, 114–120	37.53	46	97	24.5	3.2	37.5	ND	0.5	118.1	0.4	44.3	173.6
2R-3, 70–76	38.41	47	97	25.4	3.2	35.9	ND	0.7	120.8	0.5	46.0	177.5
2R-4, 73–79	39.76	49	91	25.2	3.2	35.7	ND	0.5	120.4	0.4	47.6	177.5
3R-1, 52–54	45.22	48	98	22.5	3.4	34.2	0.1	0.1	120.6	0.9	47.8	178.9
3R-2, 57–62	46.24	43	95	24.7	3.1	35.6	0.4	0.2	117.0	0.7	47.5	172.9
3R-2, 126–132	46.96	46	81	29.9	3.1	37.9	ND	16.5	116.3	0.4	47.6	169.0
3R-3, 41–50	47.55	46	128	24.4	2.8	46.0	ND	7.1	131.2	0.8	42.1	151.5
4R-1, 12–19	49.42	49	120	12.8	2.7	43.3	ND	0.3	126.6	0.9	37.9	148.9
4R-1, 69–74	49.99	44	121	21.5	2.7	42.3	0.2	2.8	121.8	0.4	38.5	142.6
4R-2, 28–34	50.90	46	128	19.7	2.8	42.5	ND	0.7	125.1	0.6	39.2	143.3
5R-1, 61–70	51.91	47	124	20.0	2.7	43.9	ND	0.4	127.2	0.6	39.2	148.1
200-1224E-												
3R-2, 51–53	28.90	48	93	22.0	3.1	37.8	ND	ND	121.2	0.5	45.6	175.0
200-1224F-												
1R-2, 133–136	30.47	49	89	22.9	3.3	37.0	0.5	0.8	121.5	0.4	48.7	174.8
1R-4, 46–49	32.55	47	89	25.0	3.2	37.3	ND	0.9	122.7	0.4	46.4	177.5
1R-4, 61–62	32.70	48	90	39.9	3.3	33.9	ND	12.2	132.1	0.8	46.2	176.3
1R-4, 118–120	33.27	49	91	16.2	3.2	35.7	0.1	0.9	117.0	0.8	45.8	171.3
1R-5, 57–59	34.09	60	93	50.7	3.4	43.5	ND	51.4	139.2	0.7	47.8	177.9
2R-1, 14–17	39.84	53	92	36.1	3.2	36.0	0.1	18.3	136.2	0.1	45.9	176.9
2R-1, 91–93	40.81	88	97	45.8	3.3	158.2	0.5	6.8	143.1	0.5	46.6	177.8
2R-3, 10–12	42.72	50	94	26.3	3.4	37.2	ND	5.7	119.7	0.8	48.6	181.8
2R-4, 138–140	45.14	50	84	18.3	3.2	36.2	ND	0.3	121.9	0.8	47.0	180.9
3R-1, 10–13	47.40	46	93	23.3	3.1	34.7	ND	0.2	117.9	0.4	48.1	175.0
3R-1, 90–95	48.20	56	82	23.2	3.5	52.4	0.0	0.2	125.5	0.7	48.8	183.8
3R-3, 90–93	50.93	55	128	25.0	3.0	44.5	ND	14.4	131.3	0.3	41.7	152.3
4R-1, 75–77	57.15	44	121	19.8	2.8	42.9	0.1	3.6	117.7	0.4	38.9	142.0
4R-2, 84–86	58.14	46	123	19.9	2.9	43.0	ND	3.1	119.2	0.5	40.4	147.4
4R-3, 1–3	58.81	52	129	15.8	2.8	41.4	ND	1.6	124.1	0.6	38.4	144.2
4R-3, 134–136	60.14	46	125	20.8	2.7	41.8	3.7	0.5	121.8	0.8	39.9	143.4
4R-5, 120–122	62.21	45	126	22.9	2.8	43.2	0.4	0.6	123.9	0.6	39.4	146.0
4R-6, 24–27	62.72	45	149	15.5	2.4	44.3	1.0	5.8	118.7	0.9	38.4	133.3
5R-1, 93–96	66.83	41	147	51.3	2.2	46.8	0.3	4.9	149.2	0.3	41.3	138.3
6R-1, 97–99	75.97	43	144	35.2	2.0	33.6	ND	14.1	127.7	0.5	37.3	128.3
7R-1, 97–99	85.47	43	143	137.1	2.2	42.4	ND	3.7	140.6	0.6	39.1	133.3
8R-1, 108–111	94.68	47	150	34.0	2.1	40.3	ND	5.9	131.0	0.1	40.1	134.0
9R-1, 46–49	103.16	46	140	30.5	2.1	40.1	ND	8.7	129.7	0.1	38.0	132.5
10R-1, 125–129	113.05	52	88	59.5	2.5	53.6	0.1	5.6	167.5	0.0	43.6	148.9
11R-1, 119–122	122.29	77	98	27.3	2.4	45.4	ND	9.4	135.8	0.2	40.4	141.7
12R-1, 46–48	128.96	70	99	61.3	2.6	46.0	ND	2.9	167.6	0.7	45.9	147.5
13R-1, 22–24	133.74	39	59	25.4	4.0	22.1	ND	1.5	122.5	0.4	55.9	222.2
14R-1, 114–116	144.34	46	67	23.7	3.8	34.0	ND	18.6	122.4	0.4	53.8	213.6
14R-2, 66–72	145.26	50	56	20.9	3.6	27.1	0.0	1.1	115.9	0.0	54.7	203.9
15R-1, 95–97	153.35	52	68	19.3	3.7	29.6	ND	0.7	115.8	0.5	53.4	202.7